JOURNAL OF SOLID STATE CHEMISTRY 30, 107–119 (1979)

Magnetic and Spectroscopic Investigation of Partially Reduced Vanadium Pentoxides. II. β'-$Cu_xV_2O_5$*

F. Y. ROBB AND W. S. GLAUNSINGER†

Department of Chemistry, Arizona State University, Tempe, Arizona 85281

Received June 28, 1978; in revised form November 3, 1978

The magnetic, electron paramagentic resonance (EPR), infrared (ir), and optical properties of β'-$Cu_xV_2O_5$ have been measured and interpreted. Magentic susceptibility studies indicate that β'-$Cu_xV_2O_5$ undergoes a semiconductor → metal transition near $x = 0.60$. For $x \leq 0.40$, the magnetic data interpreted in terms of a ligand-field model in which the octahedral $^2T_{2g}$ term of V^{4+} is split by the combined perturbations of axial distortion and spin–oribt coupling, with the result that the $^2T_{2g}$ term is split into a magnetic ground level, a weakly magentic intermediate level, and a magnetic highest level. The results of the magnetic analysis further support the transition to metallic behavior with increasing x. The EPR spectra are motionally narrowed by electronic hopping at low temperatures, and the g-tensor and linewidth data are in good agreement with the magnetic results. The ir spectra are independent of x and exhibit narrow bands at 1020 and 995 cm^{-1}, which are attributed to the stretching vibration of multiple V–O bonds. The optical spectra consist of two main bands whose peak positions shift to higher frequencies with increasing x, implying that the V^{4+}–O bond distances decrease with increasing x. The results of this study are in excellent agreement with Goodenough's interpretation of β-$M_xV_2O_5$.

Introduction

The vanadium bronzes, $-\beta$-$M_xV_2O_5$, are nonstoichiometric compounds having univalent metals M substituted into a distorted V_2O_5 framework (*1*). The structure of the β phase is depicted in Fig. 1 (*2*). The electrical and magnetic properties of these materials indicate that the ionization of M produces V^{4+} ($3d^{-1}$) and that electrical transport occurs via thermally activated hopping of the vanadium d electron among the vanadium sites (*3,4*). On the basis of structural evidence, Goodenough has suggested that this d electron occupies a d_{yz} orbital at site V_1 and that the hopping mechanism involves transport from V_1 to V_3 or V_1 to V_1' within a tunnel (*5*). Although Goodenough's model is consistent with a variety of experimental results, direct microscopic evidence for a V_1 site preference and transport via the V_3 subarray is lacking.

β'-$Cu_xV_2O_5$ is particularly interesting to study because it has the largest compositional range among the bronzes ($0.26 \leq x \leq 0.64$) (*6*). As illustrated in Fig. 2 and Table I, this system has a more complex structure than β-$M_xV_2O_5$, because Cu^+ can occupy two possible positions within its tetrahedral site (*7*). These two positions correspond to displacement of Cu^+ from the center of a tetrahedron toward its triangular face either above or below the mirror plane. Although the reduced symmetry results in six different vanadium sites instead of three, the principal physical arguments of Goodenough should still be applicable. Moreover, it has been

* This research was supported in part by grant DMR 75-09215 from the National Science Foundation.

† To whom to address inquiries.

0022-4596/79/100107-13$02.00/0

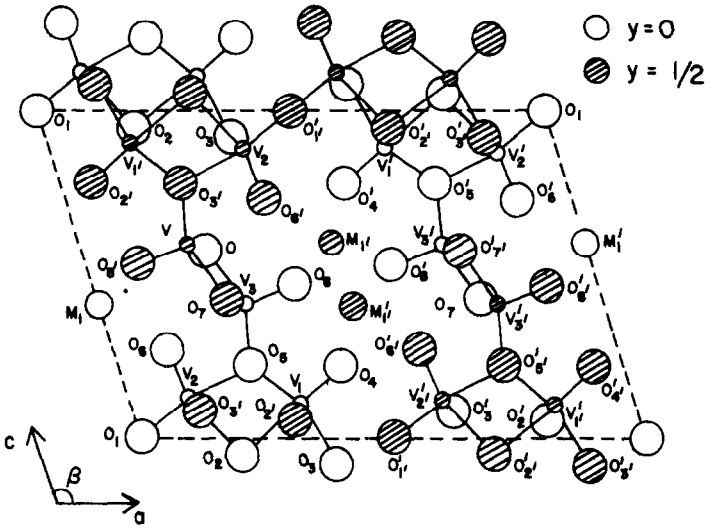

FIG. 1. Structure of β-$Ma_{0.33}V_2O_5$ projected onto the (010) plane (*2*). The M_1, M_1', $M_{1'}$, and $M_{1'}'$ sites are randomly occupied by Na^+ ions, with the restriction that two neighboring sites in the same tunnel and a–c plane cannot be occupied simultaneously.

reported that the physical properties of β'-$Cu_xV_2O_5$ are a continuous function of x and that this system exhibits a continuous semiconductor → metal transition as x increases (*6*). In this research we have studied the magnetic, electron paramagnetic resonance (EPR), infrared (ir), and optical properties of β'-$Cu_xV_2O_5$ in an attempt to test Goodenough's microscopic model for β-$M_xV_2O_5$ and to investigate further the small polaron → collective-electron transition in this unique system.

Experimental

Samples were prepared as described in the preceding paper (I). The starting materials were Johnson–Matthey specpure Cu and

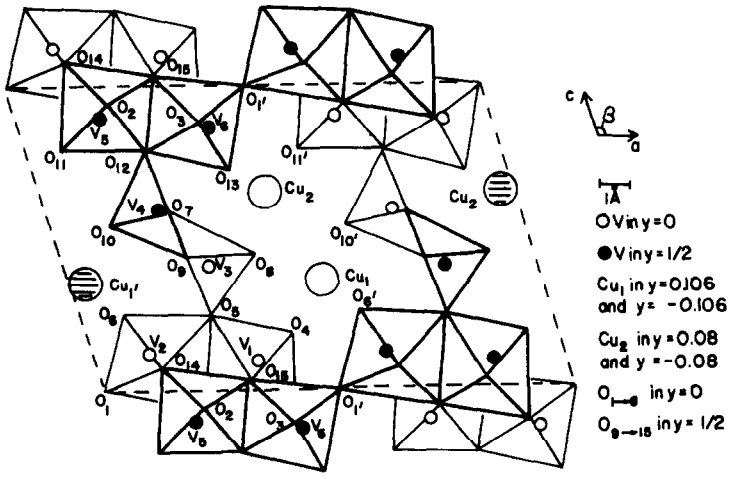

FIG. 2. Structure of β'-$Cu_{0.60}V_2O_5$ projected onto the (010) plane (*7*).

TABLE I

BOND DISTANCES IN $Cu_{0.60}V_2O_5$[a]

Bond	Distance (Å)	Bond	Distance (Å)
V_1–V_2	3.49	V_5–V_6	3.53
V_2–V_3	3.38	V_4–V_6	3.11
V_3–V_1	3.38	V_4–V_5	3.45
V_1–V_1'		V_1–V_5	3.34
V_1–V_2'		V_1–V_6	3.21
V_2–V_1'		V_2–V_5	3.19
V_3–V_3'		V_3–V_4	3.08
V_1–O_2	2.25	V_5–O_{15}	2.23
V_1–O_3	2.28	V_5–O_{14}	1.90
V_1–O_4	1.51	V_5–O_{11}	1.64
V_1–O_5	2.06	V_5–O_{12}	1.83
V_1–$O_{2'}$, O_{15}	1.92	V_5–O_2	1.91
V_2–O_1	1.89	V_6–$O_{1'}$	1.69
V_2–O_2	2.40	V_6–O_{15}	2.35
V_2–O_5	2.31	V_6–O_{12}	2.12
V_2–O_6	1.55	V_6–O_{13}	1.51
V_2–$O_{3'}$, O_{14}	1.88	V_6–O_3	1.87
V_3–O_5	1.52	V_4–O_{12}	1.91
V_3–O_7	2.12	V_4–O_9	1.84
V_3–O_8	1.60	V_4–O_{10}	1.65
V_3–$O_{7'}$, O_9	1.96	V_4–O_7	1.87
V_3–O_6	3.12	V_4–O_{13}	2.69

[a] Taken from Ref. (*7*).

V_2O_5, which contained negligible paramagnetic impurity concentrations.

Sample compositions were established by electron microprobe analysis, and the structure was checked by X-ray diffraction. Using these techniques we have found that β'-$Cu_xV_2O_5$ is stable in the range $0.26 \leq x \leq 0.67$.

The magnetic susceptibility and EPR were measured as a function of temperature as described in I. All susceptibilities were extrapolated to infinite field and corrected for the temperature-independent paramagnetism of V_2O_5 (using the value 104×10^{-6} emu/mole found in I) and the diamagnetism of the ion cores.

Infrared spectra were recorded at ambient temperature using a Beckman IR 12 spectrometer. Samples were pellets consisting of β'-$Cu_xV_2O_5$ dispersed in CsI. Optical spectra were determined at ambient and liquid-nitrogen temperatures by both KBr-pellet and diffuse-reflectance techniques using a Cary 14 spectrophotometer. In the former method a KBr pellet was placed in the reference beam to compensate for light scattering in the sample, and in the latter the samples were diluted optically by mixing them with MgO. The results obtained by both techniques were in good agreement.

We were not successful in preparing single crystals large enough for these studies. However, one partially oriented sample was prepared for EPR investigation by cementing 17 crystals together parallel to the needle (b) axis, with each having $x = 0.40 \pm 0.02$.

Results and Discussion

Magnetic Susceptibility

Figures 3 and 4 show the reciprocal susceptibility per mole of β'-$Cu_xV_2O_5$ as a function of temperature. The high-temperature data can be fitted to the Curie–Weiss law, $\chi = C/(T-\theta)$ where C and θ are the Curie and Weiss constants, respectively. The magnetic moment per atom of Cu is given by $\mu = 2.828(C/x)^{1/2}$. The magnetic parameters for β'-$Cu_xV_2O_5$ are summarized in Table II. These parameters are not in very good agreement with those found in two previous studies of β'-$Cu_xV_2O_5$ above 77°K (*6*, *8*). A possible source of this discrepancy is that the Curie–Weiss law was fitted in a different temperature range. However, the reproducibility, accurate sample compositions, and complete determination of the field dependence of the susceptibility lead us to have confidence in our data.

For $x \leq 0.50$ the magnetic moment per Cu atom is close to the spin-only value of 1.73 β, which confirms that the oxidation state of copper is +1. If Cu^{2+} were formed, then μ would be considerably larger than 1.73 β

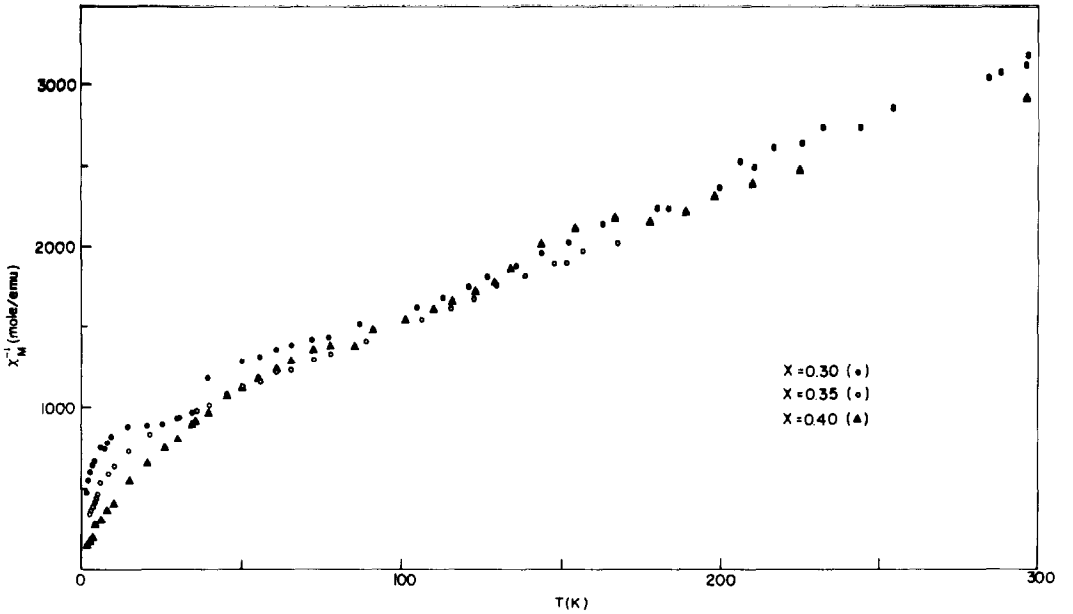

FIG. 3. Temperature dependence of the reciprocal molar susceptibility in β'-$Cu_xV_2O_5$ for $x = 0.30$ (●), 0.35 (○), and 0.40 (▲).

($\sim 5\,\beta$ for the spin-only case). The EPR results discussed in the next section show that the oxidation of the paramagnetic vanadium ion is +4. The rapid increase in calculated moment at $x = 0.60$ could be associated with the formation of Cu^{+2}, but the EPR studies rule out this possibility. Hence the sharp apparent increase in μ and $|\theta|$ and disappearance of the temperature dependence of the susceptibility above about 100°K for $x = 0.60$ signal a transition, or the onset of a transition, to the metallic state. This finding

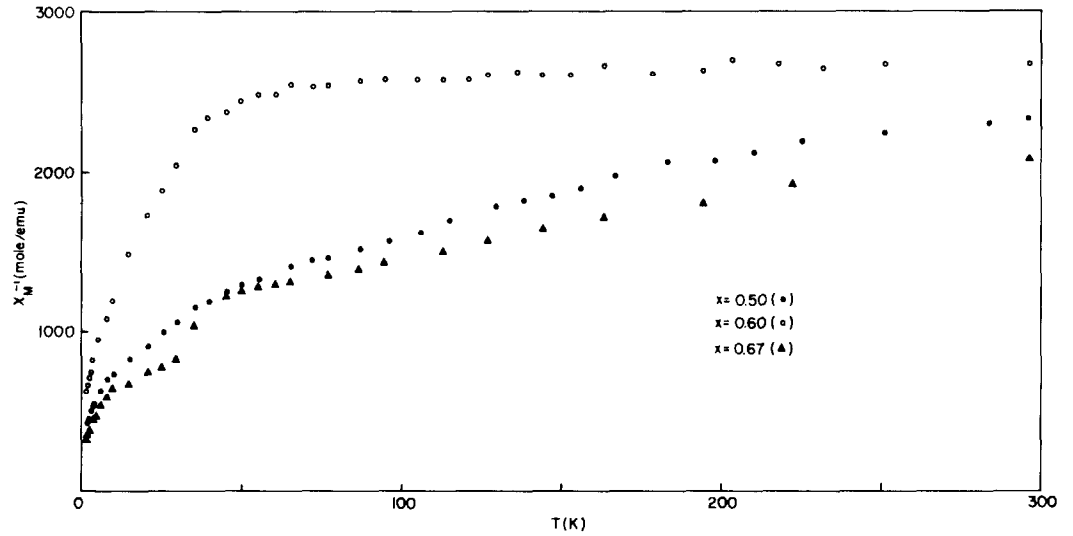

FIG. 4. Temperature dependence of the reciprocal molar susceptibility in β'-$Cu_xV_2O_5$ for $x = 0.50$ (●), 0.60 (○), and 0.67 (▲).

TABLE II

MAGNETIC PARAMETERS FOR β'-$Cu_xV_2O_5$

x	C (emu · deg mole^{-1})	θ (°K)	μ (β (atom Cu))
0.30	0.111	−78	1.72
0.35	0.111	−62	1.59
0.40	0.138	−108	1.66
0.50	0.182	−188	1.71
0.60	1.43	−3544	4.36
0.67	0.250	−258	1.73

is in good agreement with a recent single-crystal electrical conductivity study of β'-$Cu_xV_2O_5$ along the b axis, which indicated that these solids are metallic conductors for $x > 0.55$ (*9*). Further support for such a transition in β'-$Cu_xV_2O_5$ is provided by plotting the susceptibility per mole of V^{4+} as a function of x at various temperatures, as shown in Fig. 5. In agreement with a previous electrical, magnetic, and thermal study of β'-$Cu_xV_2O_5$ (*6*) the resulting straight lines all extrapolate to the common value of 480 emu/mole at $x = 0.67$, which is the theoretical insertion limit for Cu. This suggests that $Cu_{0.67}V_2O_5$ should exhibit temperature-independent paramagnetism and hence be metallic, and the large extrapolated susceptibility implies a high density of states, which is consistent with a narrow V_3 (or V_4) π^* band running parallel to the tunnels proposed by Goodenough (*5*). Unfortunately, at $x = 0.67$ Cu^{2+} EPR has been observed, and attributing the temperature dependence of the high-temperature susceptibility to Cu^{2+}, we have estimated that about 8% of the Cu in $Cu_{0.67}V_2O_5$ is present as Cu^{2+}. This suggests that Cu^{2+} should appear at $x = 0.62$; however, we have not detected any structural changes accompanying its presence. In any case no conclusions can be drawn from the interesting composition $x = 0.67$, since this composition is contaminated with Cu^{2+}.

Although the high-temperature susceptibility is nearly temperature independent for $x = 0.60$, below about 50°K χ begins to increase and at lower temperatures resembles the susceptibility trend at lower compositions. This behavior suggests that $Cu_{0.60}V_2O_5$ is barely on the metallic side of

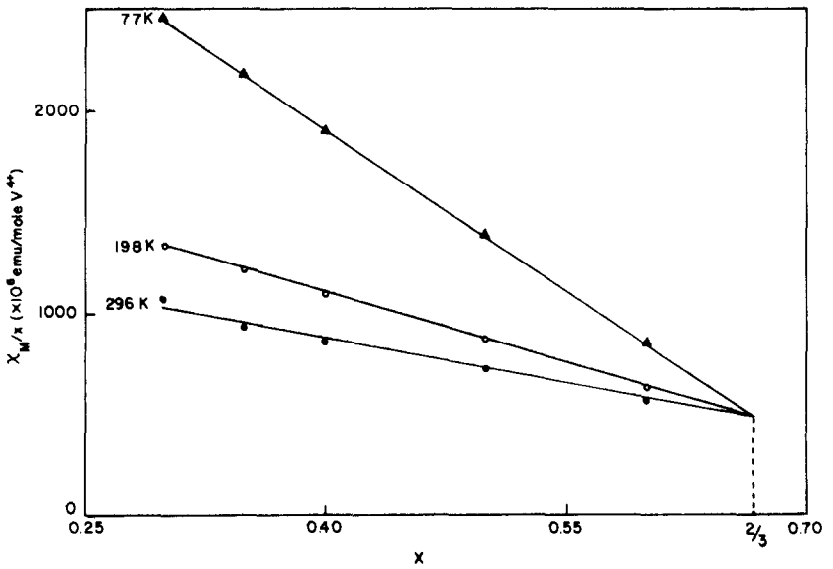

FIG. 5. Susceptibility per mole of V^{4+} as a function of composition at several temperatures in β'-$Cu_xV_2O_5$.

the semiconductor → metal transition at high temperatures, and below 50°K the interelectronic repulsions in the conduction band become sufficiently large to result in a semiconducting ground state.

Since there is no evidence for magnetic ordering down to 2°K, θ is not significant as an interaction constant, and it is useful to interpret the magnetic behavior in terms of an effective magnetic moment: $\mu_{eff} = 2.828 (\chi T)^{1/2}$. Theoretical expressions from which μ_{eff} can be calculated for a d^1 ion in an octahedral ligand field under the combined perturbations of axial distortion and spin–orbit coupling have been given in I. In semiconducting β'-$M_xV_2O_5$ the axial distortion occurs along the shortest V^{4+}–O bonds (V_1–O_4 or V_5–O_{11} in Goodenough's model (*5*)), which are directed across the tunnels for all the vanadium sites, and relative to this direction the oxygen symmetry is approximately C_{4v}. Table III summarizes the ligand-field parameters for β'-$Cu_xV_2O_5$ obtained by a least-squares fit of the theoretical moments to the experimental ones. The agreement between the theoretical and experimental moments and the resulting energy-level diagram for $Cu_{0.30}V_2O_5$ are illustrated in Figs. 6 and 7, respectively. The fit is considered to be good in view of the approximations involved, i.e., indpendent, identical V^{4+} sites having C_{4v} symmetry. In all compounds the ordering of the energy levels was $\Gamma_7(B) < \Gamma_6(E) < \Gamma_7(E)$, so that V^{4+} has a magnetic ground level, a weakly magnetic intermediate level, and a magnetic highest level. As illustrated in Fig. 8, χ obeys the Curie–Weiss law at low temperatures, and the low-temperature moment determined from the slope of the χ^{-1} vs T plot is in good agreement with calculated moment of the $\Gamma(B)$ level. For $x \leq 0.40$, the low-temperature moments are within 8% of the $\Gamma_7(B)$ moment and $|\theta| < 6$°K, which explains why magnetic ordering in these bronzes has not been observed down to 2°K. In I we

TABLE III

LIGAND-FIELD PARAMETERS FOR β'-$Cu_xV_2O_5$

x	k[a]	λ (eV)	Δ (eV)
0.30	0.8	0.018	0.002
0.35	0.7	0.020	0.004
0.40	0.6	0.026	0.009

[a] The uncertainties in k, λ, and Δ are 0.1, 0.002 eV, and 0.002 eV, respectively.

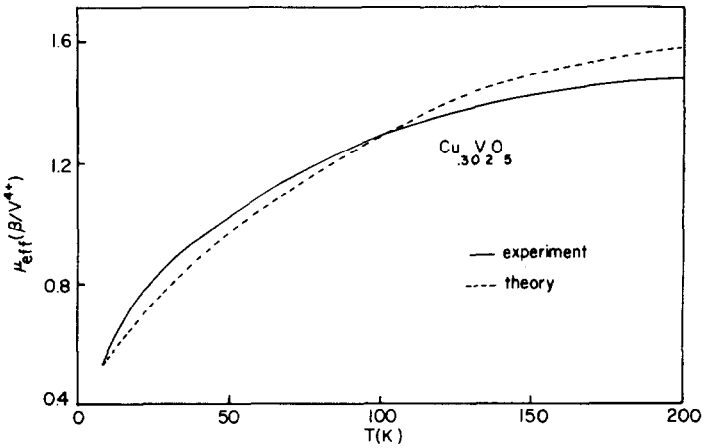

FIG. 6. Comparisons of the experimental (——) and theoretical (– – –) effective magnetic moments for $Cu_{0.30}V_2O_5$. The theoretical curve is calculated using the parameters $k = 0.8$, $\lambda = 0.018$ *eV*, and $\Delta = 0.002$ eV.

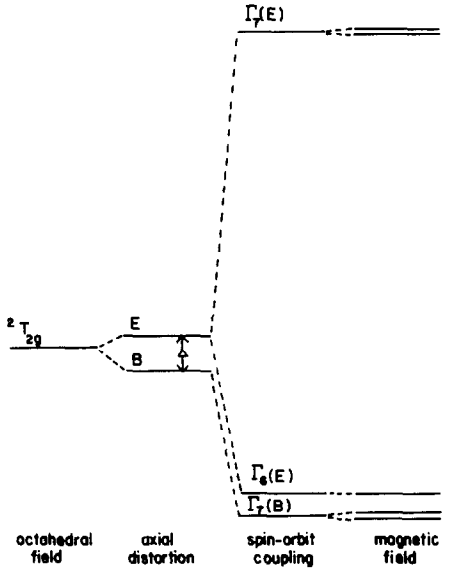

FIG. 7. Schematic energy level diagram for $Cu_{0.30}V_2O_5$.

reanalyzed the magnetic data for β-$Li_xV_2O_5$ (*10*) and found the same level sequence, which suggest that this sequence is a general one for the vanadium bronzes. This ordering of levels is consistent with the experimental data and removes Goodenough's objection to previous magnetic analyses, which incorrectly predicted a nonmagnetic ground state. Importantly, given a V_1 (or V_5) site preference, the $\Gamma_7(B)$ orbital is equivalent to Goodenough's d_{yz} orbital of a V_1 (or V_5) site.

For $x > 0.40$, it was not possible to obtain agreement between theory and experiment, which is probably due to the appreciable delocalization of the paramagnetic electron ($k < 0.6$ for β'-$Cu_{0.50}V_2O_5$).

The parameters in Table III, although subject to considerable error, do exhibit a systematic variation with composition. The small values of k indicate appreciable delocalization of the V^{4+} $3d^1$ electron onto the surrounding ligands, and the decrease in k with x reflects an increasing delocalization if the d electron as the V^{4+} concentration is increased. Such small k's are expected on the basis of Goodenough's model (*5*), since electronic transfer from V_1 (or V_5) to the V_3 (or V_4) subarray occurs via $V_1(d)$–$O_5(p\pi)$–$V_3(d)$ (or $V_5(d)$–$O_{12}(p\pi)$–$V_4(d)$) overlap, and the nearly equal V_5–O_{12} and V_4–O_{12} distances in β'-CuV_2O_5 (Table I) facilitates electronic transfer for the V_5 sites. Electronic transfer from the V_1 sites to the V_3 subarray is not favorable due to the difference in V_1–O_5 and V_3–O_5 distances (Table I) and requires a vibrational displacement of an O_5 ion toward V_1. Since such a displacement should become easier with increasing x due to the decrease in V_3–O bonding upon formation of multiple V_3-center orbitals, k should increase with x as observed.

The spin–orbit coupling constants are lower then the free-ion value (0.031 eV) and

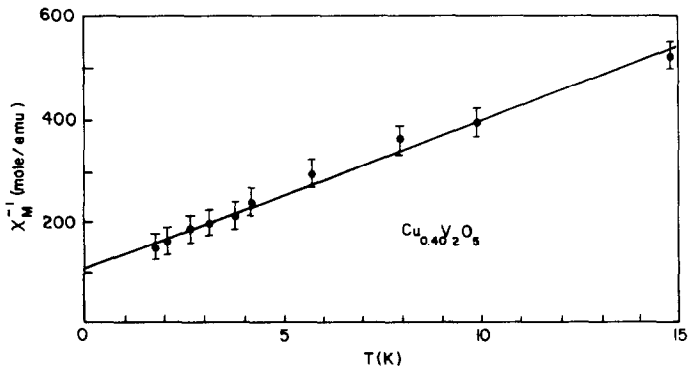

FIG. 8. Temperature dependence of the reciprocal susceptibility for $Cu_{0.40}V_2O_5$ at low temperatures. The low-temperature magnetic moment and Weiss constant are $0.83 \pm 0.98\ \beta$ and -3.8°K, respectively. The calculated moment of the ground $\Gamma_7(B)$ level is (0.79 ± 0.08).

increase with x. The reduced λ's follow from the lower effective nuclear charge of vanadium caused by covalent V^{4+}–O bonding. λ for $Cu_{0.30}V_2O_5$ is nearly equal to that for $VO(H_2O)_5^{2+}$, where the low value of λ has been attributed to vanadyl(IV)–O π bonding (*11*). The increase in λ with x indicates an increase in the effective nuclear charge of vanadium, which could result from the removal of oxide electron density by Cu^+.

The very small axial distortion can be understood in terms of the V–O distances given in Table I. In particular, the axial compression due to the short vanadyl(IV)–O bond is nearly compensated for by the axial expansion resulting from the opposite, long vanadyl(IV)–O bond. The net result is a slightly compressed C_{4v} symmetry, as indicated by the small positive Δ. The suggestion of an increase in Δ with x is interesting and, if real, could reflect changes in the axial or equatorial V^{4+}–O distances with increasing x.

Although the ligand-field model used above accounts for the main features of the magnetic behavior of β'-$Cu_xV_2O_5$ for $x \leq 0.40$, it does not explain the anomalies at 30 and 150°K for $x = 0.30$ and 0.40, respectively. Differential thermal analysis measurements have failed to detect any heat effects above 100°K for $x = 0.40$. The origin of these anomalies, as well as the failure to observe them at all compositions, is not understood at the present time.

Electron Paramagnetic Resonance

Figures 9 and 10 show typical EPR spectra of $Cu_{0.30}V_2O_5$ and $Cu_{0.67}V_2O_5$. For $x \leq 0.60$, the spectra consisted of a single Lorentzian line having $g = 1.97$, which is characteristic of V^{4+}. For $x = 0.67$, below about 120°K a second signal appears superimposed on a broad V^{4+} signal. The second signal has a g-value of 2.13, which is typical of Cu^{2+} in a tetrahedral site (*12*). The susceptibility data

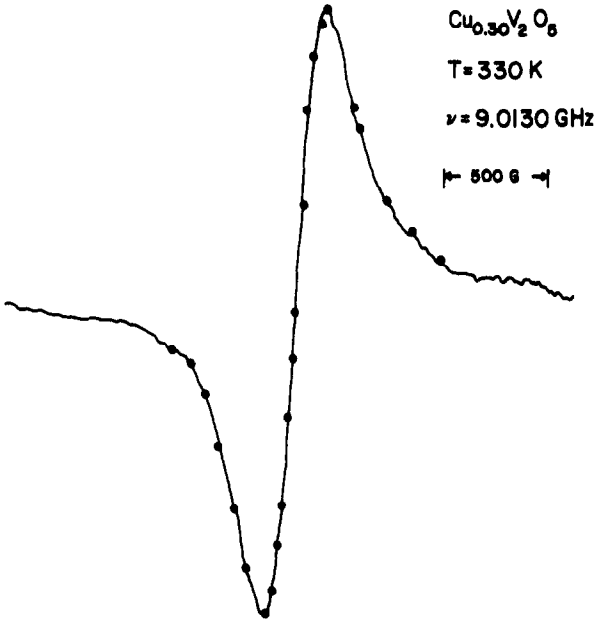

FIG. 9. EPR spectrum of $Cu_{0.30}V_2O_5$. Solid circles are values computed from Lorentzian lineshape function.

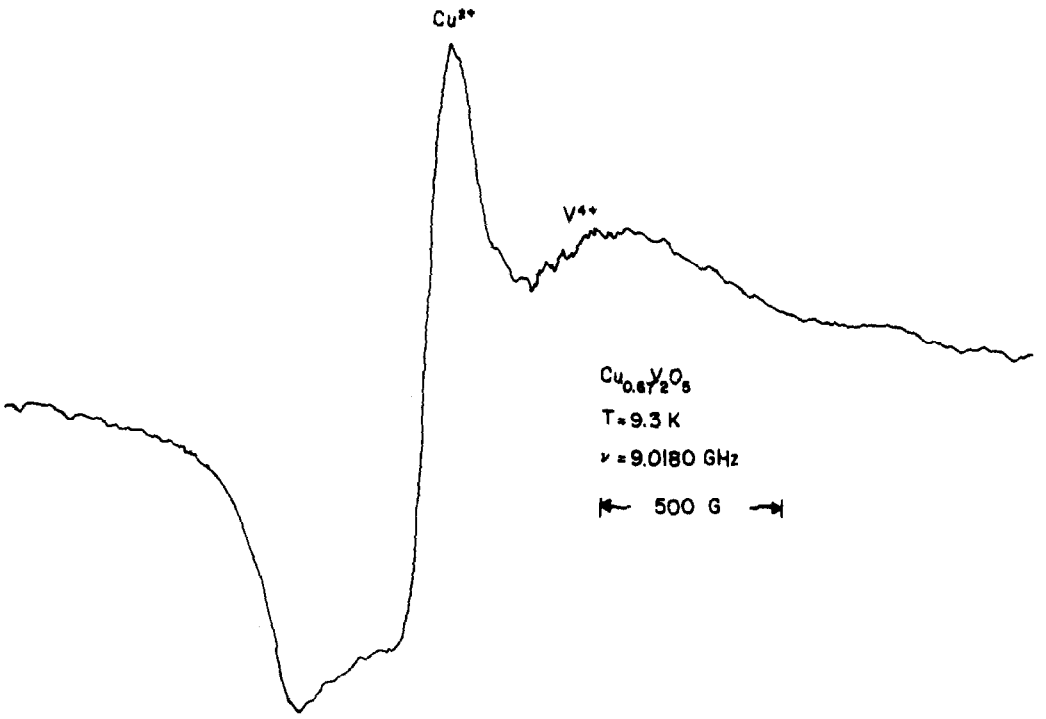

FIG. 10. EPR spectrum of $Cu_{0.67}V_2O_5$.

in the last section for $x = 0.67$ also indicate the presence of Cu^{2+}.

The EPR parameters for β'-$Cu_xV_2O_5$ are summarized in Table IV. Also shown in Table IV are the calculated dipolar widths using Eq. (6) of I with x replaced by $x^{1/2}$ and assuming a V_1–V_5 site preference. The broad signals in $Cu_{0.60}V_2O_5$ were difficult to detect. The abrupt increase in linewidth at $x = 0.60$ reinforces the susceptibility finding of a semiconductor → metal transition near this composition, since the resonance from a narrow d-band metal should be quite broad (*13*).

TABLE IV

EPR PARAMETERS FOR β'-$Cu_xV_2O_5$

x	g[a]	ΔH_{exp}[b] (G)	ΔH_d[c] (G)	$\Delta H'_d$[d] (G)
0.30	1.970	265	775	265
0.35	1.980	290	835	286
0.40	1.970	345	895	306
0.50	1.970	510	1000	342
0.60	—	~1200	1095	374

[a] The uncertainty in g is ±0.002. The signal at $x = 0.60$ was too broad for a precise determination of g.

[b] Experimental peak-to-peak linewidths are given at 298°K.

[c] Calculated dipolar peak-to-peak linewidth.

[d] Calculated peak-to-peak linewidth normalized to the experimental width of $Cu_{0.30}V_2O_5$ at 298°K.

The temperature dependence of the peak-to-peak linewidth for $Cu_{0.35}V_2O_5$ is shown in Fig. 11. The linewidth decreases with temperature up to about 50°K, exhibits a broad minimum in the range 50–200°K, and then increases with temperature above 200°K. The linewidth at low temperatures approaches the calculated dipolar value (775 G), but the sharp decrease in linewidth between 7 and 50°K is reminescent of motional narrowing, in this case by thermally activated electronic hopping between vanadium sites (*14*). Within the range of motional narrowing the lineshape should be

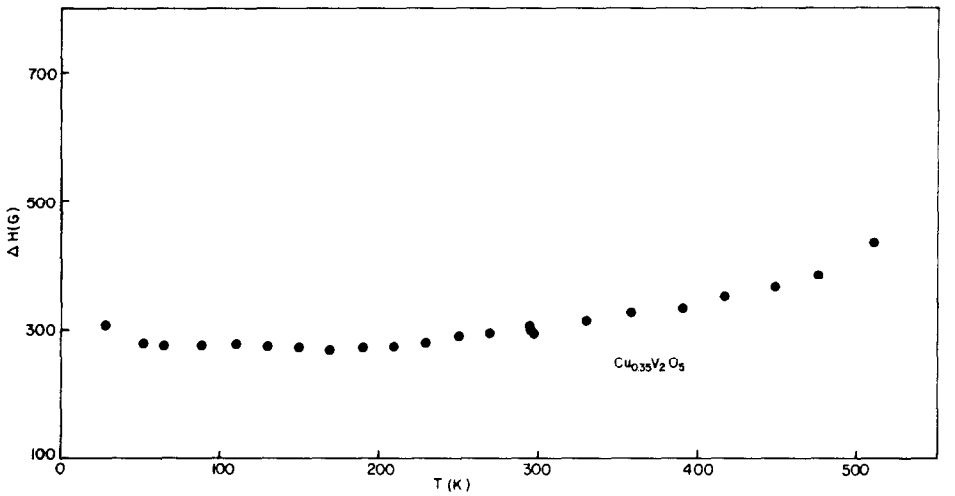

FIG. 11. Temperature dependence of the peak-to-peak linewidth in $Cu_{0.35}V_2O_5$.

Lorentzian, as observed. Using Eq. (7) of I, the activation energy E_a for electronic hopping can be estimated from the slope of semilogarithmic plot of linewidth vs reciprocal temperature. The resulting E_a's for $x = 0.30$, 0.35, and 0.40 are all about 10^{-3} eV, which is far below the experimental value of about 0.09 eV (*6*). Hence another process in addition to electronic hopping must be causing the line narrowing at low temperatures. Significantly, the temperature dependence of the linewidth over the entire temperature range can be understood qualitatively on the basis of the energy-level diagram for V^{4+} derived from the susceptibility studies discussed in the last section. The magnetic analysis of $Cu_{0.35}V_2O_5$ indicated that the energy difference between the magnetic, ground $\Gamma_7(B)$ level and the weakly magnetic, intermediate $\Gamma_6(E)$ level corresponds to about 40°K, so that in the range 7–50°K the linewidth should decrease considerably due to the reduction of the V^{4+} moment resulting from the occupancy of the $\Gamma_6(E)$ level. As the temperature is increased above 40°K, the $\Gamma_7(B)$ and $\Gamma_6(E)$ levels become nearly equally populated, and the linewidth should become independent of temperature. Since the energy separation between the $\Gamma_6(E)$ level and the magnetic, highest $\Gamma_7(E)$ level corresponds to about 350°K, as the temperature is increased above about 200°K the linewidth should begin to increase as a result of the increase in V^{4+} moment due to occupancy of the $\Gamma_7(E)$ level. Hence, as in I the sharp decrease in linewidth at low temperatures probably reflects both electronic hopping and occupation of the $\Gamma_6(E)$ level, the broad minimum at intermediate temperatures is associated with the nearly equal population of the $\Gamma_7(E)$ and $\Gamma_6(E)$ levels, and the increase in linewidth at high temperatures results from occupation of the $\Gamma_7(E)$ level. The linewidth vs temperature plots for $Cu_{0.30}V_2O_5$ and $Cu_{0.40}V_2O_5$ exhibit the same qualitative features as $Cu_{0.35}V_2O_5$ and can also be understood qualitatively on the basis of the energy-level diagram derived from the susceptibility studies. The excellent agreement between the susceptibility and EPR studies for $x \leq 0.40$ lends strong support to the magnetic analysis of the last section. The very weak signals at higher compositions prevented a precise determination of the temperature dependence of the linewidth.

A partially oriented single-crystal study of $Cu_{0.40}V_2O_5$ was conducted at 35°K by

mounting 17 crystals along their b axes to obtain an acceptable signal-to-noise ratio. The g-values parallel and perpendicular to the b axis are $g_b = 1.978 \pm 0.001$ and $g_{a,c} = 1.963 \pm 0.001$, respectively. Assuming that V^{4+} has axial symmetry, using the fact that $g = 1.970$ for powdered $Cu_{0.40}V_2O_5$ (Table IV), and noting that the unique magnetic axis, which corresponds to the shortest V–O bond, lies in the a–c plane, we calculate $g_\parallel = 1.948$ and $g_\perp = 1.978$, where $g_\parallel$ and $g_\perp$ are the g-values parallel and perpendicular to the shortest V–O bond. In terms of the Ballhausen–Gray molecular-orbital treatment for vanadyl complexes (*11*), these g-values are consistent with a V_1 (or V_5) d_{yz} ground level, as also found by the magnetic analysis of the last section.

Infrared Spectra

The infrared spectrum of $Cu_{0.35}V_2O_5$ at 298°K is shown in Fig. 12. The narrow, high-frequency bands at 1020 and 995 cm^{-1} are characteristic of the stretching vibration of multiple V–O bonds (*15*), and the lowest-frequency band probably arises from the longest V–O bonds. The peaks at intermediate frequencies are possibly due to vibrations of polymeric V–O chains (*16*). According to Goodenough (*5*), the V–O bond distances for triple and double bonds in vanadium bronzes are ≤ 1.58 Å and between 1.58 and 1.89 Å, respectively. In this case, reference to Table I indicates that the four V–O bonds having lengths <1.55 Å probably result in the band at 1020 cm^{-1}, and the four V–O bonds lying in the range 1.60–1.69 Å probably produce the 995-cm^{-1} band. Unfortunately, the peak positions do not change with composition, so that we did not observe the expected low-frequency shift in peak positions with increasing x. Such insensitivity to the environment of the metal ion is commonly observed in other vanadyl complexes (*15*).

Optical Spectra

The fact that optical spectra of vanadyl complexes are more sensitive to ligand-field environment than ir spectra (*15*) and are

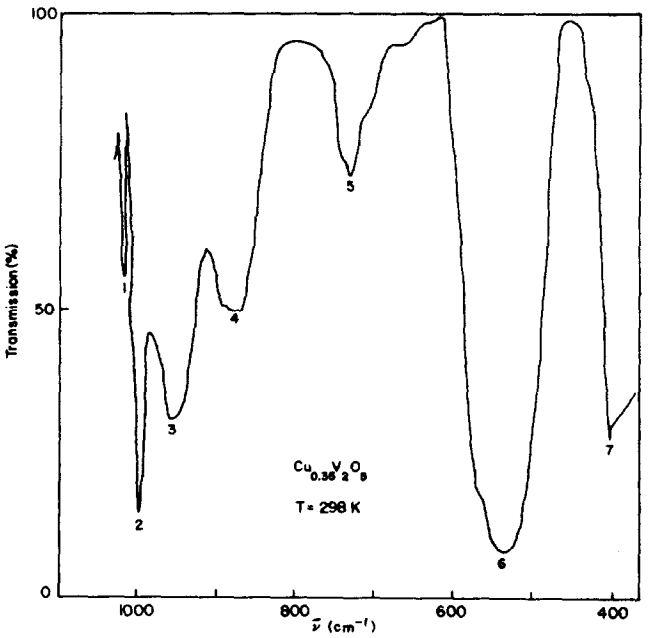

FIG. 12. Infrared spectrum of $Cu_{0.35}V_2O_5$.

specific for V^{4+} motivated us to investigate the optical spectra of β'-$Cu_xV_2O_5$. The optical spectra for $x \approx 0.35$, 0.40, 0.50, and 0.60 are displayed in Fig. 13, and the band maxima at 298°K are given in Table V. Two bands are clearly resolved in all compounds at 298°K, and for convenience we shall refer to these as bands I (between 8000 and 10 000 cm^{-1}) and II (between 13 000 and 16 000 cm^{-1}). In addition, there is a broad, intense charge-transfer band centered at 29 000 cm^{-1}.

The optical spectra in Fig. 12 resemble those obtained for a variety of vanadyl (IV) complexes (*15*), which are commonly interpreted in terms of the molecular-orbital scheme of Ballhausen and Gray (*11*) depicted in Fig. 14. In analogy to vanadyl(IV) complexes, it is tempting to assign bands I and II to the $b_2 \rightarrow e_\pi^*$ and $b_2 \rightarrow b_1^*$ transitions, respectively. The third, broad, high-frequency band is assumed to originate from the charge-transfer transitions $e_\pi \rightarrow b_2$ and $e_\pi \rightarrow e_\pi^*$. In this model the ligand-field splitting 10 Dq is equal to the $b_2 \rightarrow b_1^*$ transition energy.

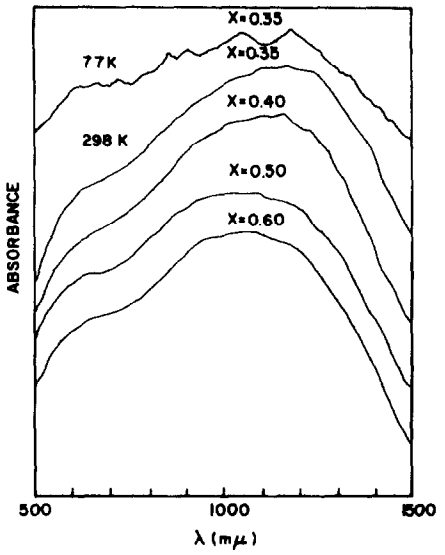

FIG. 13. Optical absorption spectra of β'-$Cu_xV_2O_5$

TABLE V

OPTICAL BAND MAXIMA FOR β'-$Cu_xV_2O_5$ AT 298°K

x	ν_{max} (cm^{-1})
0.30	8 200
	13 800
0.35	8 450
	14 300
0.40	8 900
	14 700
0.50	9 500
	15 400
0.60	9 800
	16 100

The magnetic and EPR data for β'-$Cu_xV_2O_5$ show that the ground b_2 level is equivalent to $\Gamma_7(B)$ and the e_π^* level is split into the $\Gamma_6(E)$ and $\Gamma_7(E)$ levels. However, the splitting of the $^2T_{2g}$ term by the axial field and spin-orbit coupling is so small that in a first approximation the $^2T_{2g}$ levels can be considered to be degenerate. In this case we tentatively assign bands I and II to the $^2T_{2g} \rightarrow b_1^*$ and $^2T_{2g} \rightarrow 1a^*$ transitions, with 10 Dq being approximately equal to the transition energy of band I. In any event, the high-frequency shift in the peak positions of bands I and II with increasing x indicates a significant increase in octahedral ligand-field splitting as x is increased, which in turn implies that the $V^{4+}-O$ bond distances decrease with increasing x. In particular, a decrease in the V_1–O_5 separation as x is increased would facilitate electronic transfer to the V_3 subarray, which, according to Goodenough's model (*5*), should cause a decrease in the activation energy for conductivity, as observed experimentally (*6*). As pointed out by Goodenough (*5*), the energy required for an O_5 ion displacement toward a V_1 ion is lowered by the formation

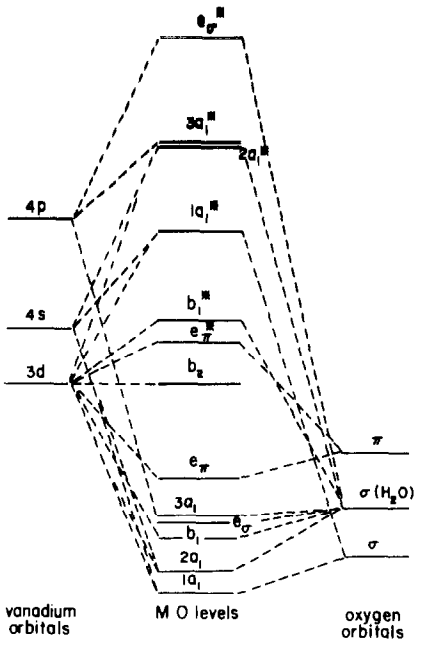

FIG. 14. Energy-level diagram for $VO(H_2O)_5^{2+}$, which has compressed C_{4v} symmetry (*11*). Vanadium orbitals are on the left, oxygen orbitals are on the right, and the molecular orbitals are in the center. The unpaired electron is in the b_2 level.

of multiple V_3-center orbitals and concomitant decrease in individual V_3–O bonding.

In the optical spectra at 298°K in Fig. 12 there is a suggestion that band I may be composed of other bands. The spectrum of $Cu_{0.35}V_2O_5$ recorded at 77°K in Fig. 13 clearly shows that both bands I and II are split into a number of components. Although all of the components are not resolved at 77°K, the splittings are usually in the range 1000–1300 cm^{-1}. Since the splitting occurs in both bands and has a value in the range of the vanadyl(IV)–O stretching vibration, the origin of the observed splittings is probably vibronic. However, the possibility that the splittings are electronic in origin cannot be ruled out. In fact, the question of whether the observed band splittings in vanadyl(IV) complexes in general are vibrational or electronic in origin is unresolved (*17*).

Conclusions

The results of this study support the view that β'-$Cu_xV_2O_5$ undergoes a semiconductor → metal transition near $x = 0.60$ and are in complete accord with Goodenough's model of β-$M_xV_2O_5$ (*5*). The magnetic and optical data indicate that small atomic displacements do occur with increasing x, and detailed single-crystal X-ray studies as a function of x are required to determine their direction and magnitude. Such measurements are now in progress in this laboratory.

Acknowledgements

The authors gratefully acknowledge Dr. P. Courtine for assistance in obtaining and interpreting the infrared and optical spectra.

References

1. M. J. SIENKO. *Advan. Chem. Ser.* **39**, 224 (1963).
2. A. D. WADSLEY, *Acta Crystallogr.* **8**, 695 (1955).
3. M. J. SIENKO AND J. B. SOHN, *J. Chem. Phys.* **44**, 1369 (1966).
4. J. H. PERLSTEIN AND M. J. SIENKO, *J. Chem. Phys.* **48**, 174 (1968).
5. J. B. GOODENOUGH, *J. Solid State Chem.* **1**, 349 (1970).
6. A. CASALOT AND P. HAGENMULLER, *J. Phys. Chem. Solids* **30**, 1341 (1969).
7. J. GALY, J. DARRIET, A. CASALOT, AND J. B. GOODENOUGH, *J. Solid State Chem.* **1**, 339 (1970).
8. A. POLACZEK, K. DYREK, AND E. POLACZKOWA, *Bull. Acad. Pol. Sci.* **20**, 705 (1972).
9. G. VILLENEUVE, H. KESSLER, AND J. P. CHAMINADE, *J. Phys. (Paris)* **10**, C4-79 (1976).
10. H. KESSLER AND M. J. SIENKO, *J. Solid State Chem.* **1**, 152 (1970).
11. C. J. BALLHAUSEN AND H. B. GRAY, *Inorg. Chem.* **1**, 111 (1962).
12. R. E. DIETZ AND H. STURGE, *Phys. Rev.* **132**, 1559 (1963).
13. B. W. HOLLAND, "Colloque Ampere XIV," p. 468, North-Holland, Amsterdam (1967).
14. G. SPERLICH, *Z. Phys.* **250**, 335 (1972).
15. J. SELBIN, *Chem. Rev.* **65**, 153 (1965).
16. C. G. BARRACLOUGH, J. LEWIS, AND R. S. NYHOLM, *J. Chem. Soc. (London)*, 3552 (1959).
17. T. R. ORTOLANO, J. SELBIN, AND S. P. MCGLYNN, *J. Chem. Phys.* **41**, 262 (1964).